Applied Mathematics and Computational Intelligence
Volume 15, No. 2, 2026 [13 – 32]

Dual Solutions of Stagnation Point of Carbon Nanotubes Across a Permeable Stretching/Shrinking Cylinder

Nur Fatin Hamiza Mohd Ayob[1*] and Norfifah Bachok[2]

[1]Department of Mathematics dan Statistics, Faculty of Science, University Putra Malaysia, 43400 UPM Serdang Selangor, Malaysia.
[2]Institute for Mathematical Research, Universiti Putra Malaysia, 43400 UPM Serdang Selangor, Malaysia.

* Corresponding author: fatinhamiza99@gmail.com

Received: 19 September 2025
Revised: 22 September 2025
Accepted: 7 February 2026

ABSTRACT

This study aims to investigate the presence of carbon nanotubes (CNTs) on the stagnation point flow and heat transfer over a stretching/shrinking cylinder with the effects of suction/injection. The findings highlight for understanding and optimizing flow and heat transfer with significant influence of suction and stagnation effects on the boundary layers in carbon nanotube-based nanofluids involving shrinking or stretching surfaces. Two types of carbon nanotubes are used which are single-walled (SWCNTs) and multi-walled (MWCNTs) with water or kerosene as the base fluid. The governing partial differential equations are converted into the ordinary differential equations by similarity transformation, which are then solved the equations numerically by using the bvp4c solver in MATLAB software. The effect on local skin friction and Nusselt numbers, velocity and temperature profile for nanoparticle volume fraction, curvature parameter, magnetic parameter and suction parameter are discussed and illustrated in graphical forms. The results indicate a range of parameters yielding dual solutions. It is determined that the curvature parameter and the suction effect could widen the range of solution due to it reduces the boundary layer separation. Furthermore, SWCNTs have a higher heat transfer rate compared to MWCNTs. Besides, kerosene exhibits a higher velocity and heat transfer rate than water as a base fluid.

Keywords: Stagnation point flow, MHD, heat transfer, carbon nanotubes, dual solutions, stretching/shrinking cylinder, suction/injection effects

1 INTRODUCTION

The study of boundary layer flow over stretching and shrinking has recently become a focus of growing research due to its wide applications in industrial and engineering fields, such as polymer processing, extrusion, cooling technologies, and biomedical systems. These processes often involve fluid motion near surfaces that either extend or contract, creating unique flow behaviors in the systems, including carbon nanotube (CNT)-based nanofluids, which exhibit enhanced thermal conductivity relative to conventional nanofluids. Stretching surface refers to a plane extending outward, inducing flow in the adjacent fluid, while a shrinking surface causes flow toward a fixed point. Nandi et al. [1] examined the stagnation point flow of methanol (CH_3OH)-based nanofluid

over a permeable stretching surface embedded in a porous medium with the effects of nonlinear thermal radiation and heat generation. Similarly, Khan et al. [2] investigated the MHD flow of viscous fluid over a nonlinear stretching cylinder under velocity and thermal slip conditions. On the other hand, Zaib et al. [3] focused on the effect of thermal radiation on mixed convective flow of copper-water nanofluid past a porous shrinking cylinder with homogeneous-heterogeneous reactions.

The stagnation point flow is a specific point in a flow field where the fluid velocity is zero. At this point, the fluid particles decelerate to a stop as they approach the solid surface. Bachok and Ishak [4] investigated a stagnation-point flow towards a nonlinearly stretching/shrinking sheet immersed in a viscous fluid. Beside, Wong et al., [5] studied of the steady two-dimensional stagnation point flow of an incompressible viscous fluid over an exponentially stretching/shrinking sheet. Futhermore, Aman et al. [6] extended the work of Wong et al. [5] with presence of magnetic field. Moreover, Anuar et al. [7] evaluated the effects of magnetic field on the stagnation point flow through a nonlinear stretching/shrinking sheet in carbon nanotubes.

Heat transfer is the exchange of thermal energy between the system and its surroundings due to the temperature difference. There are three different modes of heat transfer include conduction, convection and radiation. This study is focusing on convection mode, the transfer of heat between a solid surface and a moving fluid (liquid or gas). A year ago, Khan et al. [8] examined the heat transfer of water-based nanofluid suspended with silver nanoparticles near the stagnation point flow through a convective stretching/shrinking cylinder. Magnetohydrodynamics (MHD) is known as magneto-fluid dynamics or hydromagnetic. Kesavaiah et al. [9] stated that MHD is the study of electrically conducting fluid behaviour and magnetism. Sheikholeslami at al. [10] introduced the fundamental concept behind MHD is that a magnetic field can induce a current in a moving conductive fluid, which in turn produces a force on the fluid and changes the magnetic field itself. Aziz et al. [11] analysed the velocity slip and heat generation or absorption in MHD stagnation point flow over a permeable shrinking sheet in porous medium.

A nanofluid is defined as a fluid containing nanometer-sized particles, knows as nanoparticles (Gupta et al.,[12]). Carbon nanotubes are one of nanoparticles nanofluid that made of carbon atoms with a diameter as small as one nanometre or nanoscale (Dai and Hongjie, [13]). According to Radhamani et al. [14], carbon nanotubes are incredibly lightweight but stronger than steel, have exceptional tensile strength, high thermal conductivity, excellent electrical conductivity and exhibit unique optical properties due to their nanostructure and strength of the bonds between carbon atoms. This remarkable properties are valuable in many technological fields, such as electronics, optics, composite materials, nanotechnology and other applications of material science. So, Hayat et al. investigated the stagnation point flow of carbon nanotubes over an impermeable stretching cylinder with homogeneous-heterogeneous reactions [15], with mass transfer and slip effects [16] and with the effects of thermal radiation [17]. Then, the stagnation and heat transfer of carbon nanotubes over an exponentially stretching/shrinking sheet in the presence of homogeneous-heterogeneous reactions that studied by Anuar et al., [18]. Moreover, Allaw et al. [19] investigated the analysis of unsteady stagnation point of carbon nanotubes through exponential permeable stretching/shrinking sheet with the impacts of slip.

Suction is a widely used technique for controlling the boundary layer, aimed at minimizing energy losses within flow channels. Its application plays a vital role in improving performance in areas such as aerodynamics and space-related technologies (Halima et al., [20]). According to Yao et al. [21], suction or injection is a mechanical effect and controls lose energy in the boundary layer region by reducing the surface drag. Moreover, suction is applied to increase the efficiency of diffuser with a high compression ratio of the working fluid by preventing or delaying boundary layer separation. Mansur et al. [22] proposed a mathematical model to investigate the magnetohydrodynamic stagnation point flow of nanofluid over a stretching/shrinking sheet with suction effect. Then, Norzawary et al. explored the stagnation point flow in carbon nanotubes with suction or injection effects by a nonlinear [23] and linear [24] stretching/shrinking sheet.

Recent experimental and numerical studies have shown that the thermal performance of both single-wall and multi-wall carbon nanotubes (CNTs) can be significantly enhanced when applied in heat exchangers. Additionally, fluid flow over a cylinder represents a fundamental concept in fluid mechanics and has critical applications in various engineering domains. The study of flow around bluff bodies, such as cylinders, is particularly relevant in offshore and marine engineering, including applications like marine pipelines. It also plays an important role in structural engineering applications, such as chimneys, long-span bridges, transport vessels, high-rise buildings, towers, columns, heat exchangers, and suspension cables. In such systems, it is essential to reduce vibration risks, as well as drag and lift forces acting on the structures, to prevent potential damage or failures (Doreti et al. [25]). To further improve thermal efficiency around cylindrical structures, additional effects such as surface suction and stagnation point flow have been widely explored. The application of suction at the surface is particularly effective in controlling the boundary layer thickness, reducing flow separation, and minimizing drag, which in turn enhances the overall heat transfer characteristics. However, stagnation point flow plays a key role in increasing local heat transfer rates due to the high pressure gradients generated near the surface. Although CNT-based nanofluids are known for their superior thermal conductivity, limited studies have investigated their interaction with suction and stagnation flow conditions around permeable surfaces. This highlights the need for further research to understand how these effects influence the momentum and thermal boundary layers, especially when dealing with advanced nanofluids like single-wall or multi-wall carbon nanotubes. Thus, this study is conducted to explore the stagnation point flow and heat transfer over permeable stretching/shrinking cylinder in carbon nanotubes with suction/injection effect.

2 MATHEMATICAL FRAMEWORK

The boundary layer flow of single-walled carbon nanotubes (SWCNTs) and multi-walled carbon nanotubes (MWCNTs), water or kerosene as base fluid over a stretching/shrinking cylinder with radius, R at constant temperature, T_w and ambient temperature, T_∞ where $T_w > T_\infty$. Figure 1 illustrates the physical model of stretching and shrinking cylinder.

In the figure 1, the coordinates (x, r) represent cylindrical polar coordinates, where x and r

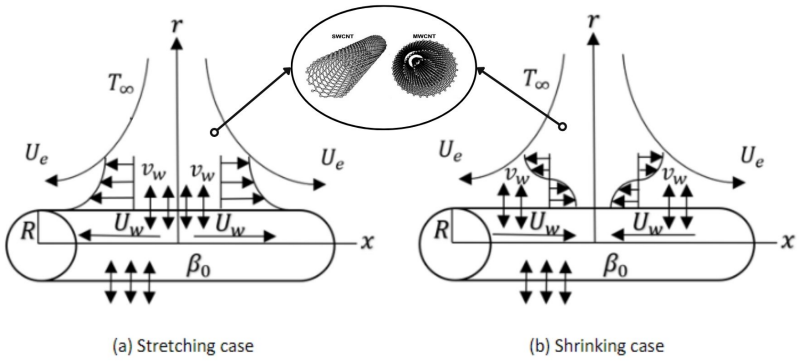

Figure 1 : The Physical model of Stretching and Shrinking Cylinder

correspond to the axial and radial directions, respectively. The velocity of stretching/shrinking cylinder is given as $U_w = \frac{c}{L}x$ and free stream velocity is $U_e = \frac{a}{L}x$ where L is length of the cylinder while a and c are constants. In addition, v_w is defined as the velocity of surface mass transfer, while β_0 is defined the ratio between fluid pressure and the square of the magnetic field strength. The fluid flow is described by the following governing equations [26]:

$$\frac{\partial}{\partial x}(ru) + \frac{\partial}{\partial r}(rv) = 0 \tag{1}$$

$$u\frac{\partial u}{\partial x} + v\frac{\partial u}{\partial r} = U_e\frac{\partial U_e}{\partial x} + \frac{\mu_{nf}}{\rho_{nf}}\left[\frac{\partial^2 u}{\partial r^2} + \frac{1}{r}\frac{\partial u}{\partial r}\right] - \frac{\sigma_{nf}\beta_0^2}{\rho_{nf}}(U_e - u) \tag{2}$$

$$u\frac{\partial T}{\partial x} + v\frac{\partial T}{\partial r} = \frac{k_{nf}}{(\rho C_p)_{nf}}\left[\frac{\partial^2 T}{\partial r^2} + \frac{1}{r}\frac{\partial T}{\partial r}\right] \tag{3}$$

with assumptions of boundary conditions (BCs) [27]:

$$u = U_w, v = V_w, T = T_w \quad at \quad r = R(x)$$

$$u \to U_e, T \to T_\infty \quad at \quad r \to \infty \tag{4}$$

The component of velocity for x and y are called u and v respectively. The subscript of nf represents nanofluids. The thermal diffusivity of nanofluids is denoted as $\frac{k_{nf}}{(\rho C_p)_{nf}}$ where k_{nf} and $(\rho C_p)_{nf}$ are thermal conductivity and heat capacity of nanofluid. $\frac{\mu_{nf}}{\rho_{nf}}$ defined as kinematic viscosity, where μ_{nf}

and ρ_{nf} are the viscosity and density of the nanofluid. Moreover, $\frac{\sigma_{nf}\beta_0^2}{\rho_{nf}}$ known as a magnetic field, where σ_{nf} is the conductivity of the nanofluid. The similarity transformations of Eq.(1) to (3) can be written as follows [26]:

$$\eta = \frac{r^2 - R^2}{2R}\left(\frac{a}{\nu_f L}\right)^{\frac{1}{2}}, \quad \psi = \left(\frac{\nu_f a}{L}\right)^{\frac{1}{2}} xRf(\eta), \quad T = T_\infty + (T_w - T_\infty)\theta(\eta) \tag{5}$$

where η is the variable of similarity and ψ is the stream function defined as $u = \frac{1}{r}\frac{\partial \psi}{\partial r}$ and $v = -\frac{1}{r}\frac{\partial \psi}{\partial x}$, which satisfies Eq.(1) by using Eq.(5). The momentum and energy equations, Eq.(2) to (3) reduce to ordinary differential equations (ODEs) as follows,

$$\frac{1}{(1-\varphi)^{2.5}(1-\varphi+\varphi\rho_{CNT}/\rho_f)}\left[(1+2\gamma\eta)f''' + 2\gamma f''\right] + ff'' \\ -f'^2 - \frac{\sigma_{nf}/\sigma_f}{1-\varphi+\varphi\rho_{CNT}/\rho_f}M[1-f'] + 1 = 0 \tag{6}$$

$$\frac{1}{Pr}\frac{k_{nf}/k_f}{1-\varphi+\varphi(\rho C_p)_{CNT}/(\rho C_p)_f}\left[(1+2\gamma\eta)\theta'' + 2\gamma\theta'\right] + f\theta' = 0 \tag{7}$$

Hence, the boundary conditions are,

$f(0) = S,\ f'(0) = \varepsilon,\ \theta(0) = 1,$

$$f'(\eta) \to 1, \theta \to 0 \quad as \quad \eta \to \infty \tag{8}$$

where M, γ and Pr are stand for magnetic field, curvature parameter and Prandtl number respectively which illustrate as $M = \frac{\sigma_f \beta_0^2 L}{\rho_f a}$, $\gamma = \left(\frac{\nu_f L}{R^2 a}\right)^{\frac{1}{2}}$ and $Pr = \frac{\nu_f}{\alpha_f}$. The subscript of CNT in Eq. (6) and (7) represents carbon nanotube. Moreover, $\varepsilon = \frac{c}{a}$ is the parameter of velocity ratio where $\varepsilon < 0$ for shrinking, $\varepsilon = 0$ for static and $\varepsilon > 0$ for stretching. S is the suction/injection parameter defined as $S = -\frac{v_w r}{\left(\frac{\nu_f a}{L}\right)^{\frac{1}{2}} R}$ which explain if $S > 0$ and $S < 0$ correspond to suction and injection.

The two interest of physical quantities in this study are the skin friction coefficient, C_f and the local Nusselt number, Nu_x [26]:

$$C_f = \frac{\mu_{nf}}{\rho_f U_e^2}\left(\frac{\partial u}{\partial r}\right)_{r=R} \tag{9}$$

$$Nu_x = -\frac{x k_{nf}}{k_f(T_w - T_\infty)}\left(\frac{\partial T}{\partial r}\right)_{r=R} \tag{10}$$

After solving, Eq.(9) and (10) can be written as

$$C_f(Re_x)^{\frac{1}{2}} = \frac{1}{(1-\varphi)^{2.5}} f''(0) \tag{11}$$

$$Nu_x(Re_x)^{-\frac{1}{2}} = -\frac{k_{nf}}{k_f}\theta'(0) \tag{12}$$

where $Re_x = \frac{U_e x}{\nu_f}$.

This study applies the mathematical model carbon nanotube given by Oztop and Abu-Nada [28]. Table 1 shows the thermophysical properties of carbon nanotube where φ is the CNTs volume fraction.

Table 1 : Thermophysical Properties of Carbon Nanotube

Thermophysical	**Carbon Nanotube**
Density	$\rho_{nf} = (1-\varphi)\rho_f + \varphi\rho_{CNT}$
Heat capacity	$(\rho C_p)_{nf} = (1-\varphi)(\rho C_p)_f + \varphi(\rho C_p)_{CNT}$
Electrical conductivity	$\sigma_{nf} = \sigma_f + \left(\frac{3\left(\frac{\sigma_{CNT}}{\sigma_f} - 1\right)\varphi}{\left(\frac{\sigma_{CNT}}{\sigma_f} + 2\right) - \left(\frac{\sigma_{CNT}}{\sigma_f} - 1\right)\varphi} \right) \sigma_f$
Thermal conductivity	$k_{nf} = k_f \left[\frac{1-\varphi+2\varphi\frac{k_{CNT}}{k_{CNT}-k_f} ln\frac{k_{CNT}+k_f}{2k_f}}{1-\varphi+2\varphi\frac{k_f}{k_{CNT}-k_f} ln\frac{k_{CNT}+k_f}{2k_f}} \right]$
Viscosity	$\mu_{nf} = \frac{\mu_f}{(1-\varphi)^{2.5}}$

Table 2 displays the thermophysical characteristics of nanoparticles carbon nanotube (SWCNTs and MWCNTs) and base fluids (water and kerosene) as in Khan et al. [29], Anuar et al. [7], and Samat et al. [30]. The elements consist of density, $\rho(kg/m^3)$, specific heat, $C_p(J/kgK)$, thermal conductivity, $k(W/mK)$ and electrical conductivity, $\sigma(S/m)$. These numbers are utilized in the computation of the numerical solutions.

Table 2 : Thermophysical Properties of Nanoparticles

Physical properties	**Base fluids**		**Nanoparticles**	
	Water	Kerosene	SWCNTs	MWCNTs
$\rho(kg/m^3)$	997	783	2600	1600
$C_p(J/kgK)$	4179	2090	425	796
$k(W/mK)$	0.613	0.145	6600	3000
$\sigma(S/m)$	5.0 x 10^{-2}	5.0 x 10^{-11}	1.0 x 10^{8}	3.5 x 10^{6}

3 NUMERICAL COMPUTATION

The MATLAB function bvp4c serves as a reliable numerical method for solving boundary value problems related to ordinary differential equations (ODEs). Hence, this study utilizes MATLAB due to the availability of the bvp4c solver, which is capable of efficiently handling these types of problems. For initiating the numerical solution, the system of ODEs, represented in Eq.(6) to Eq.(8) are converted into an equivalent system of first order differential equations through the introduction of appropriate substitution variables as outlined below:

$y(1) = f$, $y(2) = f'$, $y(3) = f''$,

$$y(4) = \theta,\ y(5) = \theta' \tag{13}$$

The momentum equation Eq.(6) can be rewrite as:

$$y(3)' = \frac{1}{1+2\gamma\eta}\left[(1-\varphi)^{2.5}\left(1-\varphi+\varphi\frac{\rho_{CNT}}{\rho_f}\right)\right.$$
$$\left.\left[-y(1)y(3)+y(2)^2+\frac{\sigma_{nf}/\sigma_f}{1-\varphi+\rho_{CNT}/\rho_f}M\left[1-y(2)\right]-1\right]-2\gamma y(3)\right] \tag{14}$$

The energy equation Eq.(7) can be rewrite as:

$$y(5)' = \frac{1}{1+2\gamma\eta}\left[\frac{-Pry(1)y(5)}{\frac{k_{nf}/k_f}{1-\varphi+\varphi(\rho C_p)_{CNT}/(\rho C_p)_f}}-2\gamma y(5)\right] \tag{15}$$

with boundary conditions Eq.(8) as follows:

$ya(1) = S$, $ya(1) = \varepsilon$, $ya(4) = 1$,

$$yb(2) \to 1, yb(4) \to 0 \tag{16}$$

where $a = 0$ corresponds to the surface at $\eta = 0$ and $b = \infty$ represents the far field condition as $\eta \to \infty$. Code A is the code that consists of bvp4c solver in MATLAB software required to solve numerically the equation (14) and (15) with boundary conditions (16). Since the current problem has dual solutions, Code A requires two different sets of initial guesses to compute both the first and second solutions. These guesses are determined through multiple attempts, adjusting the values until the boundary conditions are satisfied and accurate results are achieved.

4 RESULTS AND DISCUSSION

Table and figures are shown to present the numerical results of this research. Table 3 shows the relative values of reduced skin friction coefficient, $f''(0)$ when $\varphi = M = 0$ and different values of ε, γ with $Pr = 6.2$, which indicates a good correlation between the current results and the results of previous studies by [31] and [26]. Thus, it is guaranteed that the fluid flow and heat transfer problems can be solved confidentially using the current numerical method.

The range of parameters used in this study is based on the work by Er and Bachok [26]. The carbon nanotubes (SWCNTs and MWCNTs) are considered with varying nanoparticle volume fractions, starting from $\varphi = 0.01$, to support the research objectives. The volume fraction values are selected within the range $0 \leq \varphi \leq 0.02$. For the flow control parameters, suction is set at $S = 0.2$ and injection at $S = -0.2$. The magnetic parameter M varies from 0 to 0.2, while the curvature parameter γ is considered in the range $0 \leq \gamma \leq 0.4$. Additionally, two distinct Prandtl numbers are applied, $Pr = 6.2$ for water and $Pr = 21$ for kerosene, as referred to from Oztop and Abu-Nada [28].

Table 3 : Numerical computation for $f''(0)$ when $\varphi = M = 0$ and different values of ε, γ with $Pr = 6.2$

		Aladdin and Bachok [31]		Er and Bachok [26]		Current Result	
		First	Second	First	Second	First	Second
ε	γ	Solution	Solution	Solution	Solution	Solution	Solution
	0	1.4022408		1.4022408		1.4022408	
-0.25	0.2	1.5396153		1.5396153		1.5396153	
	0.4	1.6672781		1.6672811		1.6672781	
	0	1.4956698		1.4956698		1.4956698	
-0.5	0.2	1.6705695		1.6705695		1.6705695	
	0.4	1.8307524		1.8307579		1.8307524	
	0	1.3288169		1.3288169		1.3288169	
-1.0	0.2	1.6297671	0	1.6297678	0	1.6297671	0
	0.4	1.8836185	0	1.8836185	0	1.8836185	0
	0	0.9324733	0.2336497	0.9324733	0.2336497	0.9324733	0.2336497
-1.2	0.2	1.4106102	0.0015206	1.4106125	0.0015211	1.4106102	0.0015211
	0.4	1.7423618	-0.1165759	1.7424146	-0.1165759	1.7423618	-0.1165759
-1.4	0	1.3838419	0.1797279	1.3840578	0.1797280	1.3838419	0.1797280

4.1 Influence on Reduced Skin Friction $f''(0)$ and Reduced Heat Transfer $-\theta'(0)$

Figures 2a and 2b indicate the variation of reduced skin friction $f''(0)$ and reduced heat transfer $-\theta'(0)$ for the volume fraction of nanoparticle, φ. The result of three different volume fraction of SWCNTs/water, $\varphi = 0, 0.01$ and 0.02 are presented in both figures. The unique solutions exist for $\varepsilon > 0$, while dual solutions exist for $\varepsilon_c \leq \varepsilon \leq 0$ and there is no solution exist when $\varepsilon < \varepsilon_c$. The critical value of each increment, $\varphi = 0, 0.01$ and 0.02 is $\varepsilon_c = -1.3900, -1.3901$ and -1.3901 respectively. From that we observed when the volume fraction of nanoparticle increase, the range of solutions increases. The increase in volume fraction of nanoparticle can significantly influence the existence and behavior of the solution. Besides, the increment of volume fraction nanoparticles will decrease the reduced skin friction and reduced heat transfer. This is because the addition in the volume fraction of nanoparticle makes the viscosity of fluid to increase.

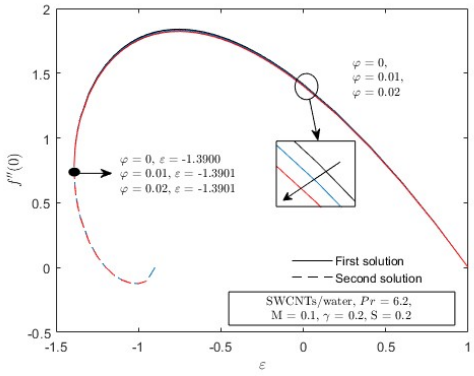

(a) Reduced skin friction, $f''(0)$

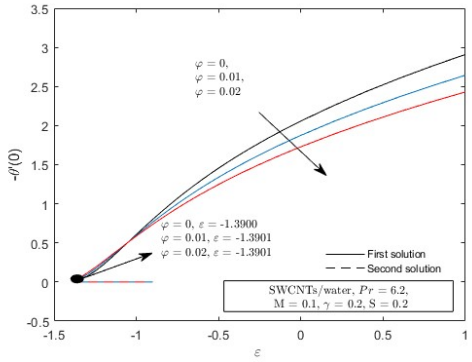

(b) Reduced heat transfer, $-\theta'(0)$

Figure 2 : $f''(0)$ and $-\theta'(0)$ for various φ of SWCNTs/water

The effects of varying curvature parameter values, γ, on the reduced skin friction, $f''(0)$, and reduced heat transfer, $-\theta'(0)$, using MWCNTs/water are illustrated in Figures 3a and 3b. The results reveal that the increasing γ contributes to delaying the onset of boundary layer separation. The carbon nanotubes are seemed to accelerate the separation of boundary layer at the flat plate with $\gamma = 0(\varepsilon = -1.2578)$, compared to $\gamma = 0.2(\varepsilon = -1.3901)$ and $\gamma = 0.4(\varepsilon = -1.4997)$ which clearly occur in shrinking region where $\varepsilon < 0$. The increase of curvature parameter cause the range of dual solution becomes widen. Furthermore, when the γ value is increased, the $f''(0)$ and $-\theta'(0)$ also increase. Heat transfer performance improves as the value of γ rises, by reducing the radius of curvature and the surface area of the cylinder containing carbon nanotube particles. Thus, it reduces the fluid resistance, improves the fluid velocity and flow stability, thereby increasing the rate of heat transfer.

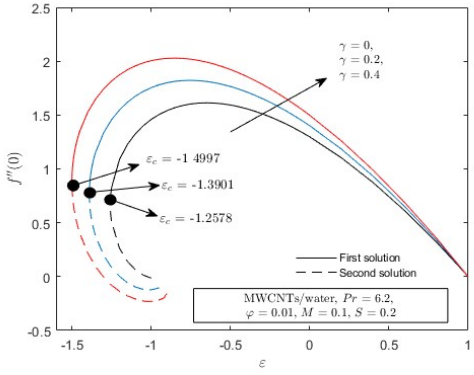

(a) Reduced skin friction, $f''(0)$

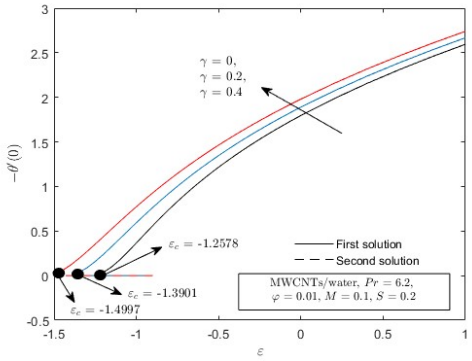

(b) Reduced heat transfer, $-\theta'(0)$

Figure 3 : $f''(0)$ and $-\theta'(0)$ for various γ of MWCNTs/water

Next, Figures 4a and 4b display the influence of different values of magnetic parameter, M on reduced skin friction $f''(0)$ and reduced heat transfer $-\theta'(0)$, with SWCNTs/kerosene. Three different values of M are used in the range of $0 \leq M \leq 0.2$. Evidently, the range of the solution narrows for $f''(0)$ and $-\theta'(0)$ with addition of M. This phenomenon aligns with the theory of Lorentz

force, which emerges from the interaction between an electromagnetic field and the movement of electrically carbon nanotubes. The magnetic field induces the Lorentz force that opposes fluid motion, slows down the movement of the fluid which consequently delays the rapid occurrence of boundary layer separation. Accordingly, it reduces convective heat transfer, resulting in weaker thermal gradient and less efficient heat transfer at the surface.

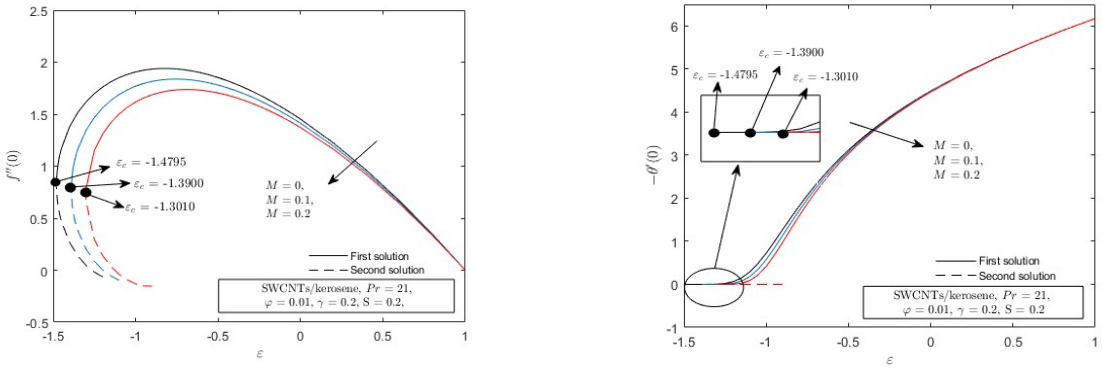

(a) Reduced skin friction, $f''(0)$

(b) Reduced heat transfer, $-\theta'(0)$

Figure 4 : $f''(0)$ and $-\theta'(0)$ for various M of SWCNTs/kerosene

Moreover, Figures 5a and 5b illustrate the graphical results of the different curvature parameters, γ, on reduced skin friction coefficient $f''(0)$ and reduced heat transfer $-\theta'(0)$ with suction effect for MWCNTs/kerosene. Figure 5a shows the dual solution are observed in the shrinking case ($\varepsilon = -1.0$) when the suction parameter S lies within the range $S_c \leq S \leq 0.5$. The corresponding critical values of S_c for each increment of the curvature parameter $\gamma = 0, 0.2$ and 0.4 are found to be $-0.4189, -0.8507$ and -1.2791, respectively. Therefore, when the curvature parameter increases, the range of solutions also increases. Otherwise, Figure 9 shows heat transfer rate increases as the increment of γ reduces the fluid particles resistance and expands the fluid velocity.

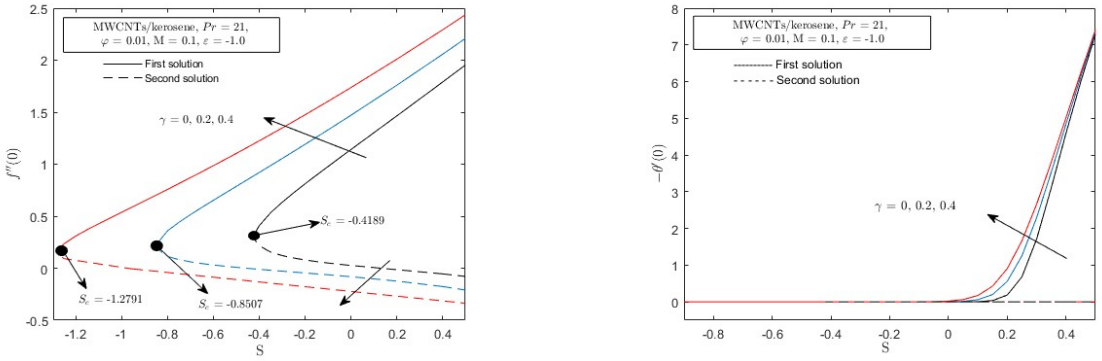

(a) Reduced skin friction, $f''(0)$

(b) Reduced heat transfer, $-\theta'(0)$

Figure 5 : $f''(0)$ and $-\theta'(0)$ for various γ with S of MWCNTs/kerosene

4.2 Influence on Local Skin Friction $C_f(Re_x)^{\frac{1}{2}}$ and Local Nusselt Number $Nu_x(Re_x)^{-\frac{1}{2}}$

Figures 6a and 6b demonstrate the effect of the curvature parameter, γ on local skin friction $C_f(Re_x)^{\frac{1}{2}}$ and local Nusselt number $Nu_x(Re_x)^{-\frac{1}{2}}$ with nanoparticle volume fraction, φ. It is concluded that, when the value of γ increases, the skin friction coefficient also increases along with the local Nusselt number. Besides, SWCNTs have higher coefficient of skin friction and local Nusselt number compared to MWCNTs. It is because SWCNTs have higher thermal conductivity due to single-layer structure compared to MWCNTs that have several graphene cylinder scattering in layers that make lower thermal conductivity.

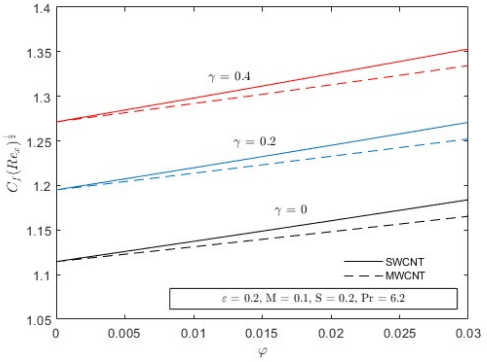

(a) Local skin friction, $C_f(Re_x)^{\frac{1}{2}}$

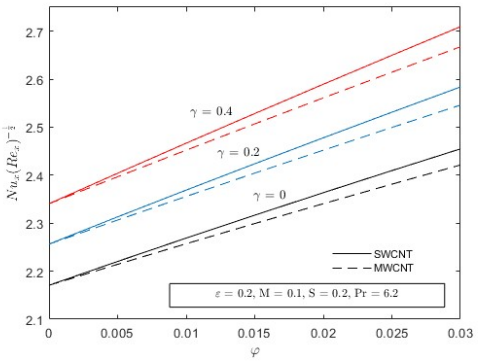

(b) Local Nusselt number, $Nu_x(Re_x)^{-\frac{1}{2}}$

Figure 6 : $C_f(Re_x)^{\frac{1}{2}}$ and $Nu_x(Re_x)^{-\frac{1}{2}}$ for various γ of CNTs/water

Then, Figures 7a and 7b present the graphical results of local skin friction $C_f(Re_x)^{\frac{1}{2}}$ and local Nusselt number $Nu_x(Re_x)^{-\frac{1}{2}}$ with nanoparticle volume fraction, φ for three distinct values of suction/injection parameter $S = -0.2, 0$ and 0.2 in stretching case $\varepsilon = 0.2$. Obviously, the graphs shown that the $C_f(Re_x)^{\frac{1}{2}}$ and $Nu_x(Re_x)^{-\frac{1}{2}}$ increase when the value of SWCNTs nanoparticle (φ) tested are increase with the increment of suction parameter. The addition of suction effect to the stretching cylinder in (SWCNTs) carbon nanotubes with water as base fluid has a significant influence. It is observed that increasing the suction parameter S enhances both skin friction and heat transfer, leading to a rise in shear stress at the surface.

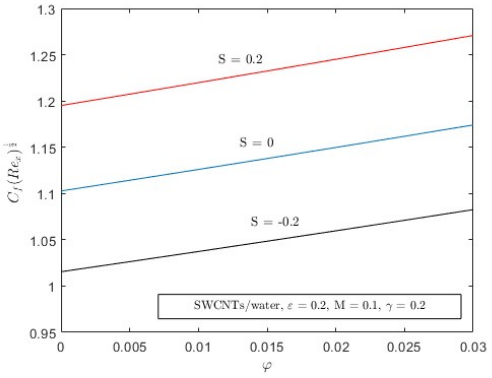

(a) Local skin friction, $C_f(Re_x)^{\frac{1}{2}}$

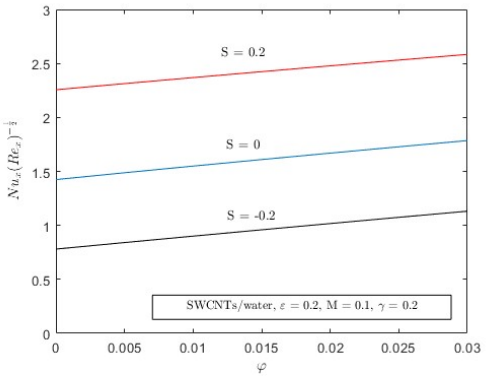

(b) Local Nusselt number, $Nu_x(Re_x)^{-\frac{1}{2}}$

Figure 7 : $C_f(Re_x)^{\frac{1}{2}}$ and $Nu_x(Re_x)^{-\frac{1}{2}}$ for various S of SWCNTs/water

In addition, the result on variation of local skin friction $C_f(Re_x)^{\frac{1}{2}}$ and local Nusselt number $Nu_x(Re_x)^{-\frac{1}{2}}$ with nanoparticle volume fraction (φ) using various value of magnetic parameter $M = 0, 0.1$ and 0.2 in stretching case $\varepsilon = 0.2$ which are illustrated in Figure 8a and 8b. As the value of nanoparticle carbon nanotubes (φ) analysed are increase for each of magnetic parameter, the value of skin friction and local Nusselt number increase. This is because the increase of nanoparticle carbon nanotubes enhances viscosity and thermal conductivity. Meanwhile, when the value of magnetic parameters increase, the local skin friction and local Nusselt number decrease. The presence of magnetic field in the tested interacts with the electrically conductive CNTs, creating a Lorentz force that opposes the fluid motion, thereby reducing the velocity gradient and heat transfer.

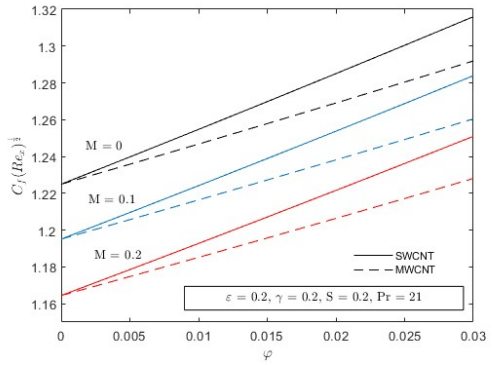

(a) Local skin friction, $C_f(Re_x)^{\frac{1}{2}}$

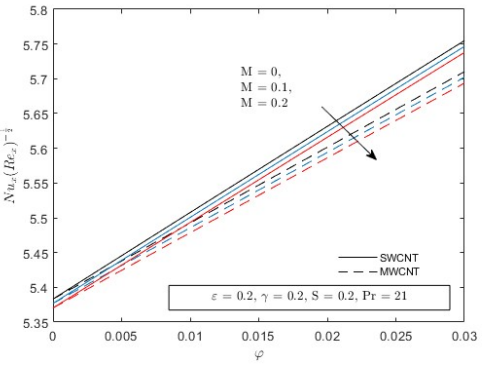

(b) Local Nusselt number, $Nu_x(Re_x)^{-\frac{1}{2}}$

Figure 8 : $C_f(Re_x)^{\frac{1}{2}}$ and $Nu_x(Re_x)^{-\frac{1}{2}}$ for various M of CNTs/kerosene

4.3 Velocity Profile $f'(\eta)$ and Temperature Profile $\theta(\eta)$

Figures 9 to 13 indicate the dual solution was proven in obtaining velocity profile and temperature profile that satisfy the boundary conditions, where solid line as first solution and dash line as second solution. Beside, the boundary layer thickness of first solution is more thin than second solution.

The nanoparticle volume fraction, curvature parameter, magnetic parameter and suction parameter effect on both profiles will be discussed in this subsection.

Figures 9a and 9b present the result of the different base fluid, water and kerosene on the velocity profiles $f'(\eta)$ and temperature profiles $\theta(\eta)$ with SWCNT in the shrinking cylinder case $\varepsilon = -1.2$. Kerosene recorded a higher velocity profile $f'(\eta)$ than water within the momentum boundary layer for both solutions. This is because kerosene has lower viscosity than water after carbon nanotube addition and suction enhances this effect, then reduces resistance to flow. Besides, kerosene heats up more quickly due to its lower heat capacity and thermal conductivity. Therefore, kerosene also reaches a higher temperature profile $\theta(\eta)$ than water.

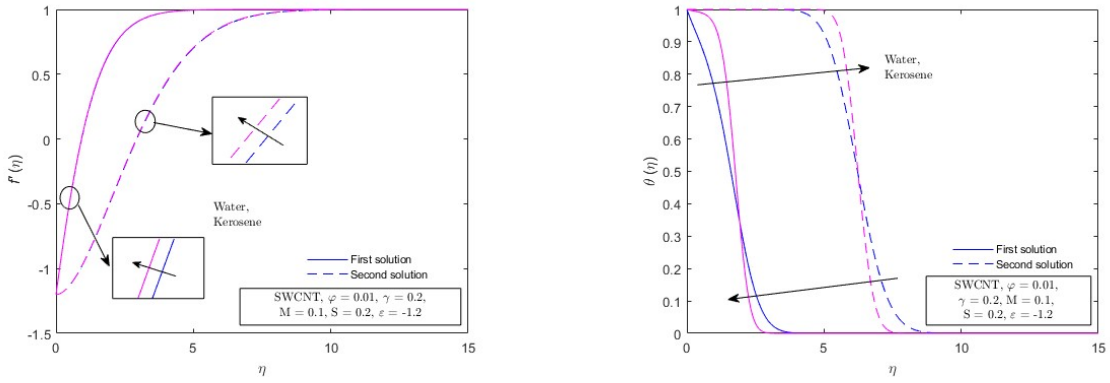

(a) Velocity profile, $f'(\eta)$ (b) Temperature profile, $\theta(\eta)$

Figure 9 : $f'(\eta)$ and $\theta(\eta)$ for different of base fluid with SWCNT

The next graphical results focus on the different volume fractions of SWCNTs nanoparticles in the value of $\varphi = 0, 0.01$ and 0.02. Therefore, Figures 10a and 10b show the effect of SWCNTs nanoparticles φ on the velocity profiles $f'(\eta)$ and temperature profiles $\theta(\eta)$ for a shrinking cylinder case $\varepsilon = -1.2$ with suction effect $S = 0.1$. The increase of nanoparticle volume fraction φ cause $f'(\eta)$ decreases significantly within the momentum boundary layer for both solutions, and $\theta(\eta)$ also decreases. Hence, the higher volume fraction of SWCNT nanoparticle $\varphi = 0.02$ have lower velocity profile and lower temperature profile compared to the other volume fraction nanoparticles.

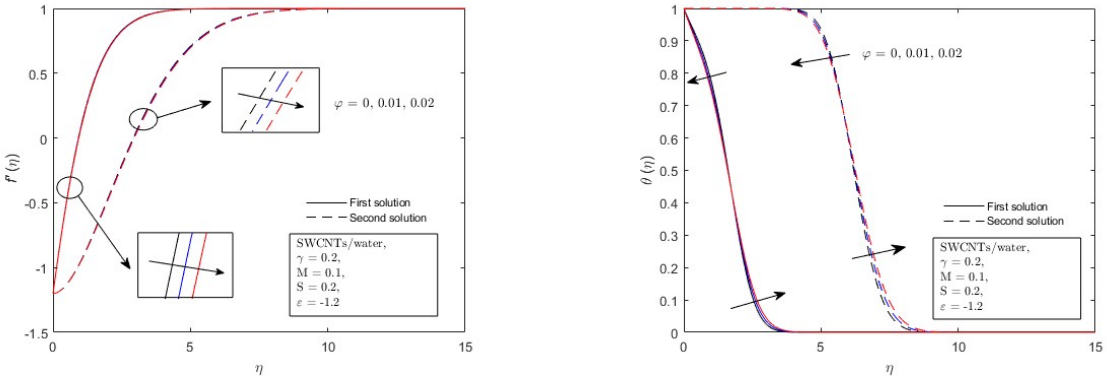

(a) Velocity profile, $f'(\eta)$ (b) Temperature profile, $\theta(\eta)$

Figure 10 : $f'(\eta)$ and $\theta(\eta)$ for various φ of SWCNTs/water

Figures 11a and 11b illustrate the influence of magnetic parameter M on the velocity profiles $f'(\eta)$ and temperature profile $\theta(\eta)$ for the SWCNTs/kerosene nanofluid in the shrinking case ($\varepsilon = -1.2$). As M increases within the range $0 \leq M \leq 0.2$, the $f'(\eta)$ decreases significantly in the first solution within the momentum boundary layer, while its increases in the second solution. Then, the temperature profile $\theta(\eta)$ rises in the first solution due to the thickening of the thermal boundary layer, but it declines in the second solution.

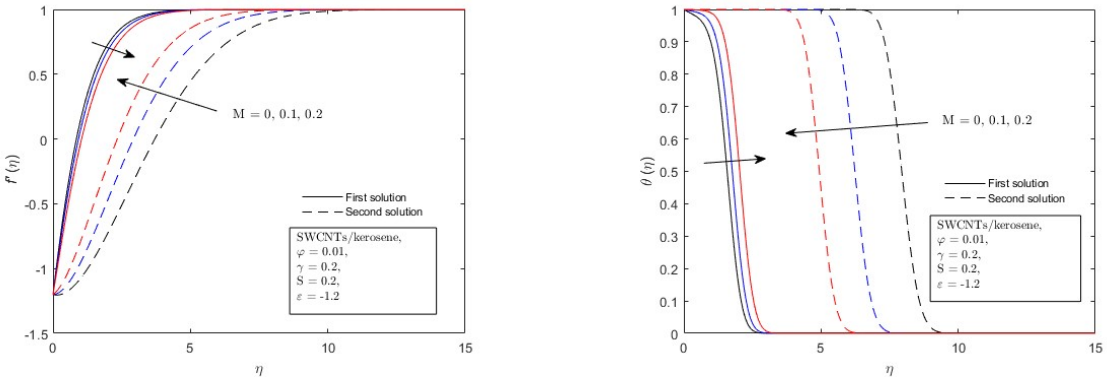

(a) Velocity profile, $f'(\eta)$ (b) Temperature profile, $\theta(\eta)$

Figure 11 : $f'(\eta)$ and $\theta(\eta)$ for various M of SWCNTs/kerosene

Moreover, the effect of curvature parameter, γ in the MWCNTs/water on the variations of velocity profiles $f'(\eta)$ and temperature profile $\theta(\eta)$ for the shrinking case have shown in Figures 12a and 12b. The graphical result clearly shows that when the curvature parameter value is increase, $f'(\eta)$ increases in first solution within the momentum boundary layer while decreases for second solution. Besides, the boundary layer region around the cylinder has a better temperature gradient when the curvature parameter is increased. It seems that the second solution has a thicker boundary layer than the first solution.

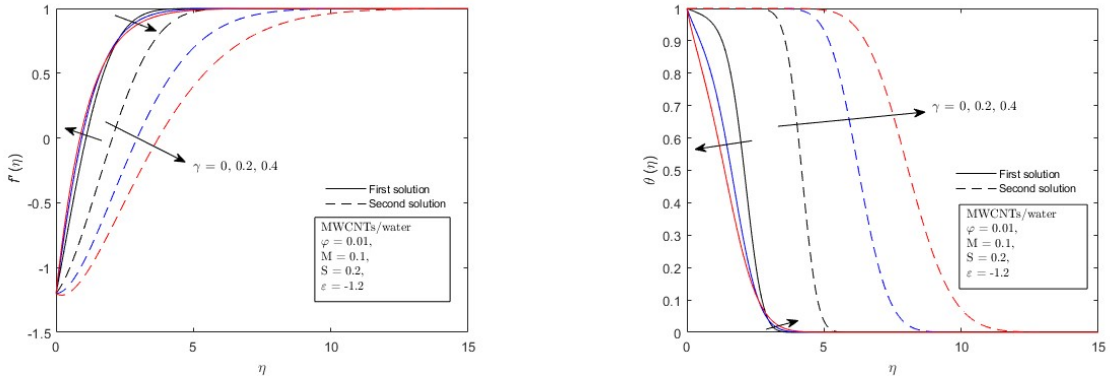

(a) Velocity profile, $f'(\eta)$ (b) Temperature profile, $\theta(\eta)$

Figure 12 : $f'(\eta)$ and $\theta(\eta)$ for various γ of MWCNTs/water

Lastly, Figures 13a and 13b present the influence of suction/injection S on the velocity profile $f'(\eta)$ and temperature profile $\theta(\eta)$ in the (MWCNTs/kerosene) carbon nanotubes with nanoparticle volume fractions, $\varphi = 0.01$ for shrinking case $\varepsilon = -1.1$. When the suction/injection effect is applied in the range of $-0.2 \leq S \leq 0.2$ in first solution, the velocity profile $f'(\eta)$ increases significantly within the momentum boundary layer but decreases for second solution. It proves that the presence of suction affects the range of duality becomes widened. Hence, the temperature profile decreases as the thickness of the thermal boundary layer thins in the first solution and increases in the second solution.

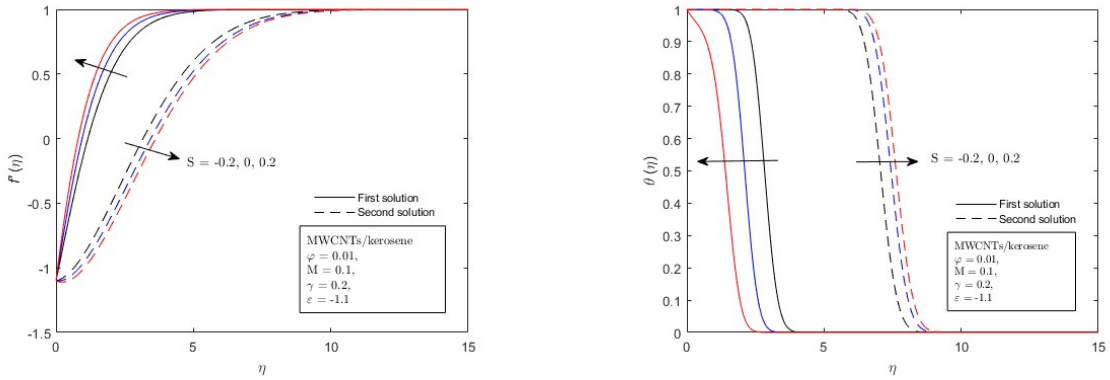

(a) Velocity profile, $f'(\eta)$ (b) Temperature profile, $\theta(\eta)$

Figure 13 : $f'(\eta)$ and $\theta(\eta)$ for various S of MWCNTs/kerosene

5 CONCLUSION

This research discussed the stagnation point flow and heat transfer of carbon nanotubes through a permeable stretching/shrinking cylinder. In the first phase of solving this problem, the partial differential equations (PDEs) transform to ordinary equations (ODEs) by applying the similarity transformation. Then, the bvp4c solver in MATLAB is used to graphically display the numerical results in particular values parameter. Therefore, the results of this study can be summed up as follows:

- The solutions for stretching/shrinking cylinder surface are unique exist for $\varepsilon > 0$, dual exist for $\varepsilon_c \leq \varepsilon \leq 0$ and no solution exist for $\varepsilon < \varepsilon_c$. The increase of curvature parameter and suction parameter widen the range of dual solutions.
- The reduced skin friction $f''(0)$ and reduced heat transfer $-\theta'(0)$ increases with an increase of the curvature parameter γ and suction parameter S.
- The reduced skin friction and heat transfer decreases when the value of magnetic parameter M increases.
- SWCNTs have higher local skin friction $C_f(Re_x)^{\frac{1}{2}}$ and local Nusselt number$Nu_x(Re_x)^{-\frac{1}{2}}$ compared to MWCNTs due to higher thermal conductivity.
- As the curvature parameter, γ and suction parameter S increase, the local skin friction and local Nusselt number increase as well.
- Kerosene has better heat transfer performance than water as base fluid.
- The boundary layer thickness of first solution is more thin than second solution.
- When the value of γ and S increase, $f'(\eta)$ decreases in first solution while increases in second solution and it is opposite to $\theta(\eta)$ for first solution and second solution.

ACKNOWLEDGEMENT

The financial support received from Universiti Putra Malaysia (GP-GPB 9784400).

REFERENCES

[1] S. Nandi, B. Kumbhakar, and S. Sarkar, "Mhd stagnation point flow of Fe3O4/Cu/Ag-CH3OH nanofluid along a convectively heated stretching sheet with partial slip and activation energy: Numerical and statistical approach," *International Communications in Heat and Mass Transfer*, vol. 130, p. 105791, 2022.

[2] M. I. Khan, M. Tamoor, T. Hayat, and A. Alsaedi, "Mhd boundary layer thermal slip flow by nonlinearly stretching cylinder with suction/blowing and radiation," *Results in Physics*, vol. 7, pp. 1207–1211, 2017.

[3] A. Zaib, A. Banerjee, and K. Bhattacharyya, "Impact of homogeneous–heterogeneous reactions on mixed convection flow of a copper–water nanofluid past a permeable shrinking cylinder with thermal radiation," *Proceedings of the Institution of Mechanical Engineers, Part E: Journal of Process Mechanical Engineering*, vol. 232, no. 5, pp. 566–578, 2018.

[4] N. Bachok and A. Ishak, "Similarity solutions for the stagnation-point flow and heat transfer over a nonlinearly stretching/shrinking sheet," *Sains Malaysiana*, vol. 40, no. 11, pp. 1297–1300, 2011.

[5] S. W. Wong, A. O. Awang, and A. Ishak, "Stagnation-point flow over an exponentially shrinking/stretching sheet," *Zeitschrift für Naturforschung A*, vol. 66, no. 12, pp. 705–711, 2011.

[6] F. Aman, A. Ishak, and I. Pop, "Magnetohydrodynamic stagnation-point flow towards a stretching/shrinking sheet with slip effects," *International Communications in Heat and Mass Transfer*, vol. 47, pp. 68–72, 2013.

[7] N. S. Anuar, N. Bachok, N. M. Arifin, and H. Rosali, "Mhd flow past a nonlinear stretching/shrinking sheet in carbon nanotubes: Stability analysis," *Chinese journal of physics*, vol. 65, pp. 436–446, 2020.

[8] M. R. Khan, V. Puneeth, M. K. Alaoui, R. Alroobaea, and M. M. M. Abdou, "Heat transfer in a dissipative nanofluid passing by a convective stretching/shrinking cylinder near the stagnation point," *ZAMM-Journal of Applied Mathematics and Mechanics/Zeitschrift für Angewandte Mathematik und Mechanik*, vol. 104, no. 3, p. e202300733, 2024.

[9] D. C. Kesavaiah, T. R. Goud, Y. Rao, and N. Venu, "Radiation effect to MHD oscillatory flow in a channel filled through a porous medium with heat generation," *Journal of Mathematical Control Science and Applications*, vol. 5, no. 2, pp. 71–80, 2019.

[10] M. Sheikholeslami and D. D. Ganji, "Ferrohydrodynamic and magnetohydrodynamic effects on ferrofluid flow and convective heat transfer," *Energy*, vol. 75, pp. 400–410, 2014.

[11] H. J. Aziz, K. Zaimi, F. Kamal, A. Asghar, S. F. Sufahani, L. A. Lund, U. Yashkun, and M. Ferdows, "Mhd stagnation-point flow towards a permeable shrinking/stretching sheet in a porous medium with velocity slip and heat generation/absorption effects."

[12] H. Gupta, G. Agrawal, and J. Mathur, "An overview of nanofluids: A new media towards green environment," *International Journal of environmental sciences*, vol. 3, no. 1, pp. 433–440, 2012.

[13] H. Dai, "Carbon nanotubes: opportunities and challenges," *Surface science*, vol. 500, no. 1-3, pp. 218–241, 2002.

[14] A. Radhamani, H. C. Lau, and S. Ramakrishna, "Cnt-reinforced metal and steel nanocomposites: A comprehensive assessment of progress and future directions," *Composites Part A: Applied Science and Manufacturing*, vol. 114, pp. 170–187, 2018.

[15] T. Hayat, M. Farooq, and A. Alsaedi, "Homogeneous-heterogeneous reactions in the stagnation point flow of carbon nanotubes with Newtonian heating," *AIP advances*, vol. 5, no. 2, 2015.

[16] ——, "Stagnation point flow of carbon nanotubes over stretching cylinder with slip conditions," *Open Physics*, vol. 13, no. 1, 2015.

[17] T. Hayat, M. I. Khan, M. Waqas, A. Alsaedi, and M. Farooq, "Numerical simulation for melting heat transfer and radiation effects in stagnation point flow of carbon–water nanofluid," *Computer methods in applied mechanics and engineering*, vol. 315, pp. 1011–1024, 2017.

[18] N. S. Anuar, N. Bachok, N. M. Arifin, and H. Rosali, "Stagnation point flow and heat transfer over an exponentially stretching/shrinking sheet in cnt with homogeneous–heterogeneous reaction: stability analysis," *Symmetry*, vol. 11, no. 4, p. 522, 2019.

[19] D. Allaw, N. Bachok, N. M. Arifin, and F. M. Ali, "Double solutions of unsteady stagnation-point of carbon nanotubes across a permeable exponential stretching/shrinking sheet," *Chinese Journal of Physics*, vol. 85, pp. 534–552, 2023.

[20] U. Halima, A. Dogondaji, and A. Sammani, "Effects of injection/suction on unsteady mhd natural convective radiative flow of heat mass transfer in a plumb frequency," *Saudi J Eng Technol*, vol. 8, no. 7, pp. 171–180, 2023.

[21] S.-W. Yao, M. Ahmad, M. İnç, I. Ahmad, M. I. Asjad, and M. Nazar, "Suction effect on MHD flow of brinkman-type fluid with heat absorption and first-order chemical reaction," *Frontiers in Energy Research*, vol. 10, p. 963583, 2022.

[22] S. Mansur, A. Ishak, and I. Pop, "The magnetohydrodynamic stagnation point flow of a nanofluid over a stretching/shrinking sheet with suction," *PLoS one*, vol. 10, no. 3, p. e0117733, 2015.

[23] N. H. A. Norzawary, N. Bachok, and F. M. Ali, "Effects of suction/injection on stagnation point flow over a nonlinearly stretching/shrinking sheet in a carbon nanotubes," *Journal of Advanced Research in Fluid Mechanics and Thermal Sciences*, vol. 76, no. 1, pp. 30–38, 2020.

[24] ——, "Stagnation point flow over a stretching/shrinking sheet in a carbon nanotubes with suction/injection effects," *CFD Letters*, vol. 12, no. 2, pp. 106–114, 2020.

[25] L. K. Doreti and L. Dineshkumar, "Control techniques in flow past a cylinder-a review," in *IOP Conference Series: materials science and engineering*, vol. 377, no. 1. IOP Publishing, 2018, p. 012144.

[26] L. X. Er and N. Bachok, "Stagnation point flow and heat transfer of hybrid nanofluid over a stretching/shrinking cylinder with suction/injection effects," *Journal of Advanced Research in Numerical Heat Transfer*, vol. 17, no. 1, pp. 14–28, 2024.

[27] N. Najib, N. Bachok, N. F. Dzulkifli, and I. Pop, "Numerical results on slip effect over an exponentially stretching/shrinking cylinder," *Mathematics*, vol. 10, no. 7, p. 1114, 2022.

[28] H. F. Oztop and E. Abu-Nada, "Numerical study of natural convection in partially heated rectangular enclosures filled with nanofluids," *International journal of heat and fluid flow*, vol. 29, no. 5, pp. 1326–1336, 2008.

[29] W. Khan, Z. Khan, and M. Rahi, "Fluid flow and heat transfer of carbon nanotubes along a flat plate with Navier slip boundary," *Applied Nanoscience*, vol. 4, pp. 633–641, 2014.

[30] N. A. A. Samat, N. Bachok, and N. M. Arifin, "Magnetohydrodynamic flow of carbon nanotubes and heat transfer over a moving thin needle: A numerical and research surface methodology," *Ain Shams Engineering Journal*, vol. 15, no. 8, p. 102833, 2024.

[31] N. A. L. Aladdin and N. Bachok, "Effects of hydromagnetic and chemical reaction over a stagnation point flow of horizontal stretching/shrinking cylinder in Ag-CuO/water hybrid nanofluid," *International Journal of Numerical Methods for Heat & Fluid Flow*, vol. 32, no. 2, pp. 660–683, 2022.